View metadata, citation and similar papers at core.ac.uk

brought to you by CORE

provided by University of New Orleans

University of New Orleans

ScholarWorks@UNO

University of New Orleans Theses and Dissertations

Dissertations and Theses

5-20-2005

Magneto-Optic Spectroscopy and Near-Field Optical Coupling in Nanoparticle Composite Materials

Damon Smith
University of New Orleans

Follow this and additional works at: https://scholarworks.uno.edu/td

Recommended Citation

Smith, Damon, "Magneto-Optic Spectroscopy and Near-Field Optical Coupling in Nanoparticle Composite Materials" (2005). *University of New Orleans Theses and Dissertations*. 246.
https://scholarworks.uno.edu/td/246

This Thesis is protected by copyright and/or related rights. It has been brought to you by ScholarWorks@UNO with permission from the rights-holder(s). You are free to use this Thesis in any way that is permitted by the copyright and related rights legislation that applies to your use. For other uses you need to obtain permission from the rights-holder(s) directly, unless additional rights are indicated by a Creative Commons license in the record and/or on the work itself.

This Thesis has been accepted for inclusion in University of New Orleans Theses and Dissertations by an authorized administrator of ScholarWorks@UNO. For more information, please contact scholarworks@uno.edu.

MAGNETO-OPTIC SPECTROSCOPY AND NEAR-FIELD OPTICAL COUPLING IN NANOPARTICLE COMPOSITE MATERIALS

A Thesis

Submitted to the Graduate Faculty of the
University of New Orleans
in partial fulfillment of the
requirements for the degree of

Master of Science
in
Applied Physics

by

Damon A. Smith

B.S., University of New Orleans

May 2005

TABLE OF CONTENTS

LIST OF FIGURES……iv

ABSTRACT……vi

CHAPTER 1: INTRODUCTION……...1

1.1 Overview and Motivation……. 1

1.2 Background on the Magneto-Optic Effect…… 2

1.3 Magneto-Optic Materials…….....3

1.4 Optics of Nanocomposite Materials……..... 3

CHAPTER 2: THEORY……5

2.1 Derivation of Polarization Parameters…….....5

2.2 Origin of the Magneto-Optic Effect…….....9

2.3 Scattering and Maxwell's Equations……...12

2.4 Particles Small Compared to the Wavelength of Light……...15

2.5 Coupled-Dipole Model (CDM) for Nanocomposite Materials……...18

2.6 CDM in a Right-Left Circular Coordinate System……20

2.7 Calculation of the Faraday Rotation……... 20

CHAPTER 3: EXPERIMENT…….....….....22

3.1 Experimental Setup for Magneto-Optic Measurements……..... 22

3.2 PEM Method of Polarization Measurement……... 23

3.3 Sample Preparation…….....25

CHAPTER 4: RESULTS AND DISCUSSION……27

4.1 Experimental Results…….. 27

4.2 Calculation of Two-Particle Geometries…… 28

4.3 Cubic Arrays of Particles…… 32

CHAPTER 5: CONCLUSION……..... 36

REFERENCES…….. 37

APPENDIX A: DIELECTRIC TENSOR ELEMENTS……... 38

APPENDIX B: MATHEMATICA PROGRAM FOR TWO-PARTICLE CALCULATIONS... 40

APPENDIX C: MATLAB PROGRAM FOR ARBITRARY PARTICLE ARRANGEMENTS……45

VITA…….. 56

LIST OF FIGURES

2.1-1 In-phase Linear Vibrations…….. 6

2.1-2 Elliptical Polarization……...7

2.1-3 Linear Polarization…….…….....8

2.1-4 Left- and Right-Circular Polarization……..... 9

2.2-1 Energy Transitions for Left and Right Circular Polarizations…….……...10

2.2-2 Polar and Longitudinal Faraday Geometries…….…… 11

2.3-1 Scattering by an Arbitrary Particle……..... 13

2.4-1 Electric Dipole……... 17

3.1-1 Experimental Coordinate System…….. 22

3.1-2 Experimental Setup……23

3.2-1 PEM Modulation……24

3.3-1 Photo of Varying Particle/PMMA Concentrations…… 25

3.3-2 TEM Image of Magnetite Nanoparticles……... 26

4.1-1 Experimental Faraday Spectra……... 27

4.1-2 Experimental Spectral Shifts……..28

4.2-1 Calculated X-Aligned Two-Particle Faraday Spectra……29

4.2-2 Calculated Y-Aligned Two-Particle Faraday Spectra……30

4.2-3 Calculated Z-Aligned Two-Particle Faraday Spectra…… 30

4.2-4 Calculated Two-Particle Spectral Shifts…… 31

4.3-1 Calculated Faraday Spectra for 2x2x2 Cubic Particle Array…….33

4.3-2 Calculated Faraday Spectra for 4x4x4 Cubic Particle Array…….33

4.3-3 Calculated Faraday Spectra for 6x6x6 Cubic Particle Array…….34

4.3-4 Calculated Cubic Array Spectral Shifts……. 34

4.3-5 Comparison of All Calculated Spectral Shifts……... 35

ABSTRACT

The Faraday rotation spectrum of composites containing magnetite nanoparticles is found to be dependent on the interparticle spacing of the constituent nanoparticles. The composite materials are prepared by combining chemically-synthesized Fe_3O_4 (magnetite) nanoparticles (8 nm diameter) and poly(methylmethacrylate) (PMMA). Composites are made containing a range of nanoparticle concentrations. The peak of the main spectral feature depends on nanoparticle concentration; this peak is observed to shift from approximately 470 nm for (dilute composites) to 560 nm (concentrated). A theory is presented based on the dipole approximation which accounts for optical coupling between magnetite particles. Qualitative correlations between theoretical calculations and experimental data suggest the shifts in spectral peak position depend on both interparticle distance and geometrical configuration.

CHAPTER 1: INTRODUCTION

1.1 Overview and Motivation

The coupling of light with structures much smaller than the light's wavelength (typically, interaction lengths less than 100 nm) is particularly relevant with the current push to fabricate photonic devices on the nanometer scale.[1] Previous studies of these optical near-field interactions have focused mostly on noble metal nanoparticles, which display resonances in the optical absorption spectrum dependent on the particle size, shape and interparticle spacing.[2] In addition, light has been shown to propagate along noble metal nanoparticle chains.[3] Here, we extend the investigations of near-field optical interactions and include a study of the *magneto-optical* properties of nanoparticles as a function of interparticle spacing. Magneto-optically active nanoparticles could have applications in the emerging field of nanophotonics, data storage or sensing.

The magneto-optical properties of films containing *dilute* concentrations of Fe_3O_4 (magnetite) particles have previously been studied.[4,5] Barnakov et al. recently reported that shifts in the Faraday rotation spectrum of magnetite/polymer nanocomposites are observed with changes in the nanoparticle size, with particle diameters ranging from 8 nm to 200 nm.[6] In this work, we report shifts in Faraday rotation peak position that are dependent on the concentration of nanoparticles in the matrix. Magnetite particles are estimated to have separations (on average) as small as a few nanometers. To explain these results, a new theory is presented based on the coupled-dipole approximation, which accounts for optical dipole-dipole coupling between the magnetite particles.

1.2 Background on the Magneto-Optic Effect

On September 13, 1845 Michael Faraday discovered what is known as the magneto-optic effect. On that day, after experimenting with polarized light transmitted through glass, he recorded the following passage in his lab notebook: "A piece of heavy glass, which was 2 in. by 1.8 in. and 0.5 of an inch thick, being a silicoborate of lead, was experimented with… when contrary magnetic poles were on the same side there *was an effect produced on the polarized ray*, and thus magnetic force and light were proved to have relations to each other. This fact will most likely prove exceedingly fertile, and of great value in the investigation of conditions of nature force."[7] After several days work, he verified that the effect of the magnet was to rotate the plane of polarization by an angle proportional to the strength of the magnet. This can be illustrated by the equation[8]

$$\theta = VHL\,, \tag{1.1}$$

where θ is the angle of rotation of the polarized light, L is the thickness of the material, H is the applied magnetic field, and V is the Verdet constant. The Verdet constant depends on the properties of the medium, the wavelength of the light, and the temperature. The Scottish physicist John Kerr discovered a similar effect in 1888. He was conducting an experiment where he examined the polarization of light, which was reflected off the pole of a polished electromagnet. Again the plane of polarization was found to rotate after reflection from the surface of the magnet. Accordingly, magneto-optics conducted by transmission and reflection is referred to as the Faraday and Kerr effect, respectively.

1.3 Applications of Magneto-Optical Materials

Since Faraday's original discovery, magneto-optic effects have proven to be an extremely significant phenomenon for both fundamental science and the development of numerous applications. Various Magneto-Optical devices have been developed which include modulators, bistable optical switches, optical isolators, magneto-optical circulators, deflectors, transparencies and displays, read heads, and low-insertion-loss magneto-optical elements for laser gyroscopes.[8] In addition to these devices, magneto-optical memories have been used extensively in the form of disks and tapes.

A wide range of magnetic materials have been studied over the last several decades. Magneto-optical materials can be divided into two main groups. The first includes metals and metal alloys, which are only partially transparent at film thicknesses less than 100 nm. These materials are typically studied using the Kerr effect and includes rare-earth-transition metal alloys, which are often used in magneto-optical disk memory systems. The other group includes the dielectric and semimagnetic materials. Magnetic dielectrics, such as ferromagnetic garnets, orthoferrites, spinel ferrites, and oxides are generally quite transparent and lend themselves for Faraday effect applications.[8]

1.4 Optics of Nanocomposite Materials

Calculations of the magneto-optic effects of nanocomposite materials are often made using effective medium theory (EMT). These calculations are made by determining the effective dielectric tensor elements by taking the volume average of the dielectric functions of the constituent materials.[9] However, EMT does not take into account optical coupling between the nanostructured elements.

Discrete-dipole approximation (DDA) calculations have been used to determine the scattering and absorption of a large variety of nanometer sized structures and geometries. The DDA replaces the structures with collections of point dipoles which interact optically. DDA methods have been used in astrophysical calculations to determine the optical cross-sections of interstellar graphite grains.[10] In addition, Lazarides et al. have used the DDA for DNA-linked gold nanoparticles, where each particle is replaced by a single dipole.[11]

In this study, we adapt the DDA calculations for determination of the magneto-optical properties of collections of nanoparticles. This allows for the first faraday effect calculations which take into account the near-field optical interactions between particles.

CHAPTER 2: THEORY

2.1 Derivation of Polarization Parameters

In order to discuss how magneto-optic effects change the polarization of light, a graphic illustration is derived that fully defines the state of polarization. The polarization of an electromagnetic monochromatic wave can be described as the behavior of the electric field vector as it moves through time, observed from a fixed point in space. The electric field vector can be broken into three independent, linear, simple-harmonic vibrations[12]

$$\vec{E} = E_x\hat{x} + E_y\hat{y} + E_z\hat{z}\,, \tag{2.1}$$

$$E_i = E_{0i}\cos(\omega t + \delta_i)\,, \tag{2.2}$$

where $i = x, y, z$, E_{0i} is the amplitude, and δ_i is the phase along the *i*th coordinate axis. Each of the linear vibrations can be broken into two collinear vibrations

$$E_i = (E_{0i}\cos\delta_i)\cos\omega t - (E_{0i}\sin\delta_i)\sin\omega t\,. \tag{2.3}$$

Additionally, the group of three oscillations represented by equation (2.3) can be broken into two subgroups. The first subgroup contains all of the $(E_{0i}\cos\delta_i)\cos\omega t$ terms and the second contains all of the $-(E_{0i}\sin\delta_i)\sin\omega t$ terms. Each subgroup represents three in-phase linear vibrations which vary in time by either $\cos\omega t$ or $-\sin\omega t$. It can be shown (fig. 2.1-1) that any two (or more) in-phase vibrations along different directions combine to form a single linear vibration that is in-phase with its component vibrations. This allows us to rewrite equation (2.3) as

$$\vec{E} = (a_1\cos\omega t)\hat{u}_1 - (a_2\sin\omega t)\hat{u}_2\,, \tag{2.4}$$

where $\hat{u}_1$ and $\hat{u}_2$ are unit vectors which represent the resultant linear vibrations of the two subgroups, and a_1 and a_2 are their respective amplitudes. If we take the plane containing the unit vectors, with γ representing the angle between the two vectors, we can define

$$\cos\gamma = \hat{u}_1 \cdot \hat{u}_2 \tag{2.5}$$

and

$$\sin\gamma = \left|\hat{u}_1 \times \hat{u}_2\right|. \tag{2.6}$$

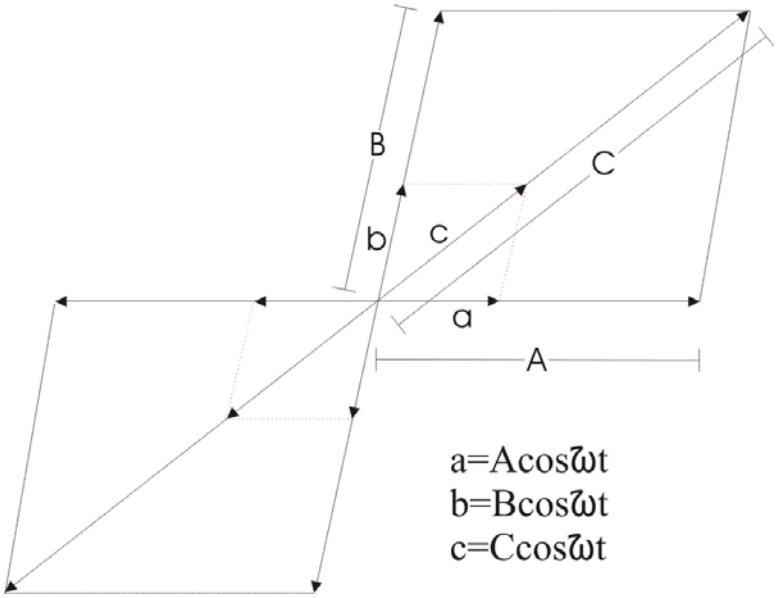

Figure 2.1-1: Two in-phase linear vibrations combine to form a third in-phase linear vibration.[12]

If we take the projections of $\vec{E}$ of equation (2.4) parallel and perpendicular to $\hat{u}_1$, we have

$$E_{\parallel} = a_1 \cos\omega t - (a_2 \cos\gamma)\sin\omega t \tag{2.7}$$

and

$$E_{\perp} = -(a_2 \sin\gamma)\sin\omega t\,. \tag{2.8}$$

With the above derived equations, it is straight forward to show that

$$\frac{E_{\parallel}^2}{a_1^2}+\frac{E_{\perp}^2}{(a_2\sin\gamma)^2}-\frac{2E_{\parallel}E_{\perp}\cos\gamma}{a_1^2}=1, \tag{2.9}$$

which is the equation of an ellipse in the plane of the unit vectors $\hat{u}_1$ and $\hat{u}_2$. Therefore, the tip of the electric field vector traces out an ellipse in the general case of a monochromatic wave (fig. 2.1-2).

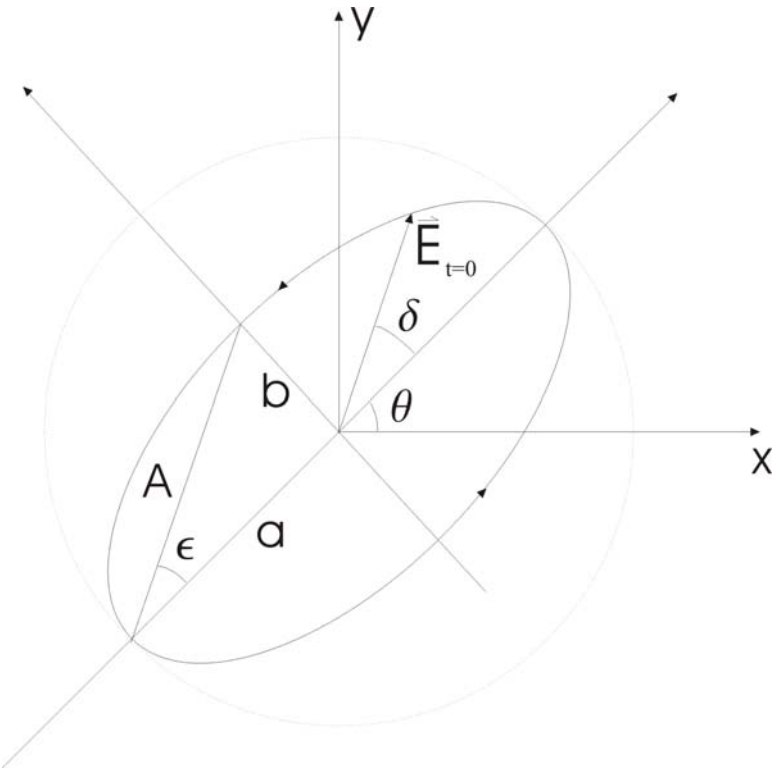

Figure 2.1-2: Diagram of elliptical polarization where θ is the rotation of the plane of polarization, η is the ellipticity, δ is the phase, and A is the amplitude of the electric field. [12]

The elliptical polarization is generally defined by the four parameters[12]:

i. azimuth θ of the major axis from a reference direction;

ii. the ellipticity η, where + and – signs refer to right- and left-handed polarizations, respectively, which defines the direction the tip of the electric field vector moves in time;

iii. the total amplitude A, where $A = \sqrt{a^2 + b^2}$;

iv. and the phase δ, which is represented by the angle between the electric field vector and the major axis a time $t = 0$.

The special case of polarization where the light is linearly polarized with an azimuth of 0^o and an ellipticity of zero is shown in figure 2.1-3. The two illustrations in figure 2.1-4 display right- and left-handed circularly polarized light with ellipticities of 45^o and -45^o, respectively.

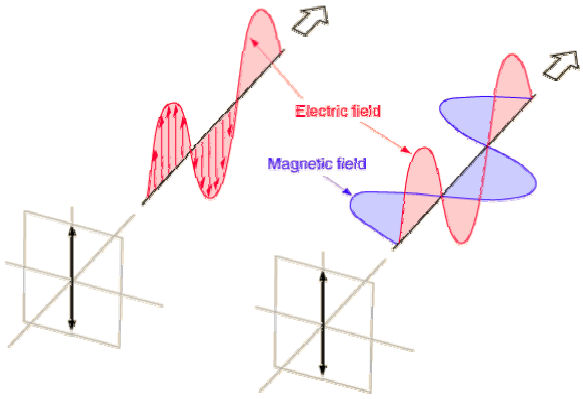

Figure 2.1-3: Illustration of the special case of linearly polarized light, where $\theta = 0^o$ and $\eta = 0^o$.

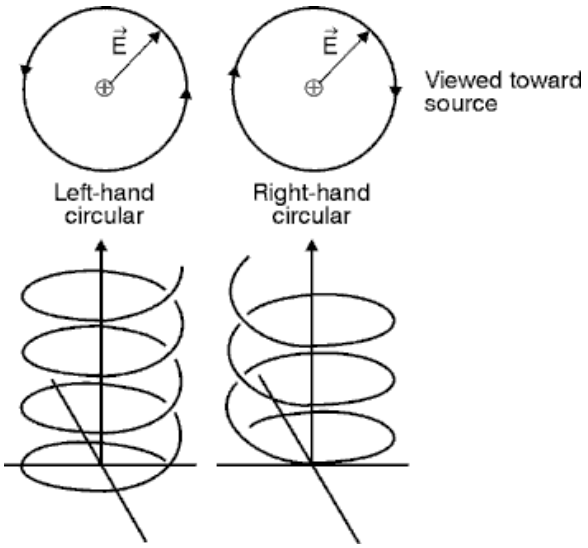

Figure 2.1-4: Illustration of left- and right-circularly polarized light, where $\eta = 45^o, -45^o$, respectively.

2.2 Origin of the Magneto-Optic Effect

Magneto-optical effects arise from a magnetic field-induced anisotropy, which manifests itself through the presence of non-symmetric, off-diagonal components of a material's dielectric tensor. These off-diagonal components are a result of different electronic transitions excited by left and right circularly polarized light.[8] In the absence of a magnetic field, the two processes are equal and no magneto-optic effect occurs (fig. 2.2-1).

The placements of the off-diagonal components within the dielectric tensor vary according to the particular orientation of the axis of propagation of incident light and the direction of the applied magnetic field. In this study, we focus on the case where the magnetic

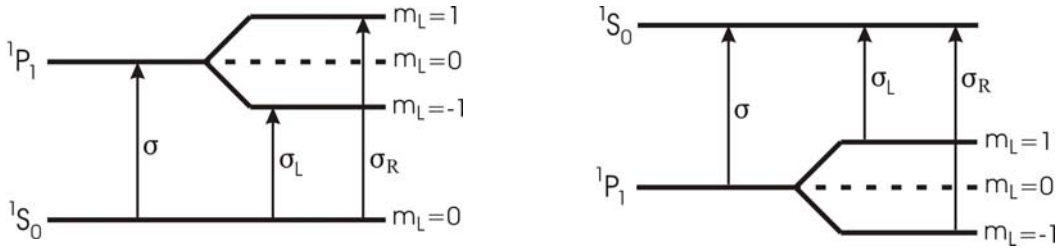

Figure 2.2-1: Energy level splittings which result in a difference in optical absorption energy for left and right circularly polarized light. σ_L indicates left circular polarization (spin -1) and σ_R indicates right circular polarization (spin +1). [8]

field is parallel to the axis of propagation of the incident radiation. This is referred to as the "polar" geometry (fig. 2.2-2) and results in a dielectric tensor of the following form[8]

$$\tilde{\varepsilon} = \begin{pmatrix} \varepsilon_{xx} & i\varepsilon_{xy} & 0 \\ -i\varepsilon_{xy} & \varepsilon_{xx} & 0 \\ 0 & 0 & \varepsilon_{xx} \end{pmatrix}, \tag{2.10}$$

where ε_{xx} is the diagonal component and ε_{xy} is the off-diagonal component. A transformation to a right-left-handed circular cylindrical coordinate system can be made with the transformation matrix[12]

$$\tilde{f} = \frac{1}{\sqrt{2}} \begin{pmatrix} 1 & 1 & 0 \\ -i & i & 0 \\ 0 & 0 & \sqrt{2} \end{pmatrix}, \tag{2.11}$$

by the matrix multiplication

$$\tilde{\varepsilon}^{rl} = \tilde{f}^{-1}\tilde{\varepsilon}\tilde{f}\,, \tag{2.12}$$

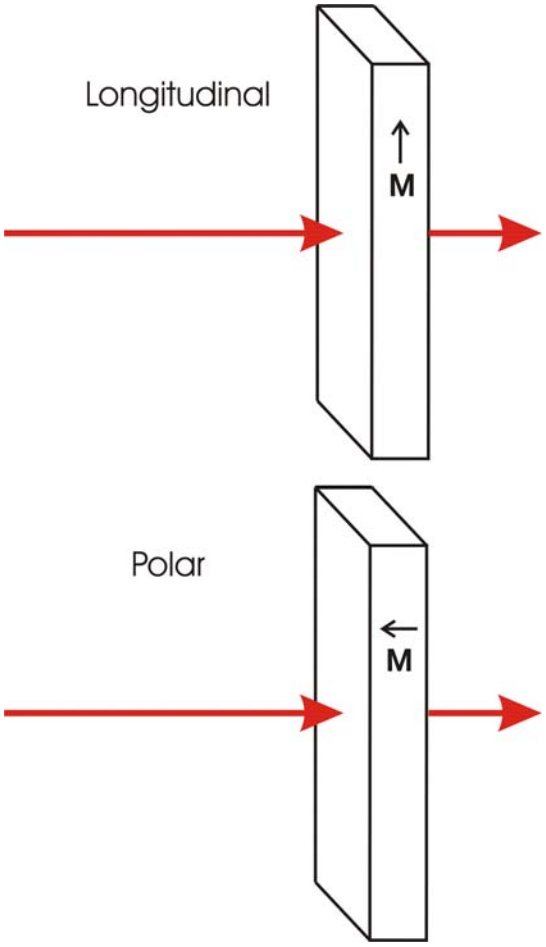

Figure 2.2-2: Polar and longitudinal geometries for transmission (Faraday) magneto-optical measurements.

polarized light, which can be written as

$$n_{\pm}^2 = \varepsilon_{xx} \pm \varepsilon_{xy}, \tag{2.14}$$

where the + and - denote the right- and left-circular index of refraction, respectively.

where the rl superscript represents the right-left-handed circular cylindrical coordinate system. With this transformation, the dielectric tensor is diagonalized

$$\tilde{\varepsilon}^{rl} = \begin{pmatrix} \varepsilon_{xx} + \varepsilon_{xy} & 0 & 0 \\ 0 & \varepsilon_{xx} - \varepsilon_{xy} & 0 \\ 0 & 0 & \varepsilon_{xx} \end{pmatrix}, \tag{2.13}$$

and displays the difference in the index of refraction for right-left handed circularly

If we write the complex index of refraction as

$$\tilde{n} = n + i\kappa, \tag{2.15}$$

the difference between the left and right circular indexes is[13]

$$\tilde{n}_+ - \tilde{n}_- = (n_+ - n_-) + i(\kappa_+ - \kappa_-) = \frac{\varepsilon_{xy}}{\sqrt{\varepsilon_{xx}}}. \tag{2.16}$$

The complex Faraday rotation angle is given by the sum of the azimuthal angle and the ellipticity

$$\Theta = \theta + i\eta = \frac{\pi}{\lambda}\left(\tilde{n}_+ - \tilde{n}_-\right). \tag{2.17}$$

The Faraday rotation is just proportional to the difference in the real parts of the index of refraction (phase difference)

$$\theta = \frac{\pi}{\lambda}\left(n_+ - n_-\right) = \frac{\pi}{\lambda}\mathrm{Re}\left[\frac{\varepsilon_{xy}}{\sqrt{\varepsilon_{xx}}}\right] \tag{2.18}$$

and the ellipticity is given by the difference in the absorption,

$$\eta = \frac{\pi}{\lambda}\left(\kappa_+ - \kappa_-\right) = \frac{\pi}{\lambda}\mathrm{Im}\left[\frac{\varepsilon_{xy}}{\sqrt{\varepsilon_{xx}}}\right]. \tag{2.19}$$

2.3 Scattering and Maxwell's Equations

Fundamentally, all optical interactions can be categorized as scattering processes in the sense that any optical process involves the absorption and re-radiation of light by ions in solids, molecules or free electrons. This absorption/re-radiation process is, of course, governed by

Maxwell's equations. For this study, we were interested in composite thin film materials in which the optically-active constituents consist of magnetic nanoparticles embedded in a transparent, nonmagnetic medium. Therefore, as a first step towards the development of a model for magneto-optic effects in this system, it is important to look at what happens to an individual particle in an electric field (fig. 2.3-1).

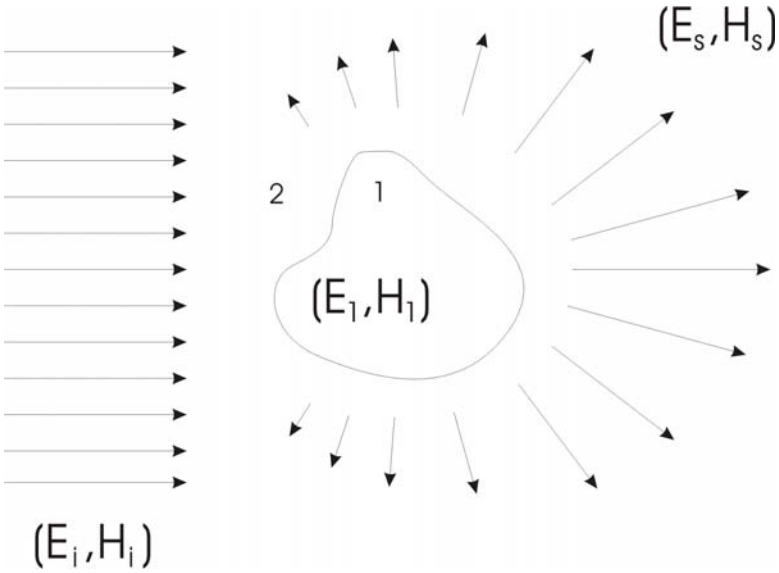

Figure 2.3-1: Scattering by and arbitrary particle in an electromagnetic field. The subscript i indicates the incident field, 1 indicates the field inside the particle, and s represents the scattered field. [14]

A particle illuminated by a beam of light can scatter light in a large variety of ways depending on its shape, size, and composition. Considering an incident field defined by the plane harmonic waves,

$$\vec{E}_i = \vec{E}_0 \exp(i\vec{k} \cdot \vec{x} - i\omega t) \tag{2.15}$$

and

$$\vec{H}_i = \vec{H}_0 \exp(i\vec{k} \cdot \vec{x} - i\omega t), \tag{2.16}$$

the field outside the particle is the sum of the incident and scattered fields[14],

$$\vec{E}_2 = \vec{E}_i + \vec{E}_s \tag{2.17}$$

and

$$\vec{H}_2 = \vec{H}_i + \vec{H}_s, \tag{2.18}$$

where $\vec{E}_s$ and $\vec{H}_s$ are the scattered electric and magnetic fields, respectively.

These fields must satisfy Maxwell's equations

$$\vec{\nabla} \cdot \vec{E} = 0, \tag{2.19}$$

$$\vec{\nabla} \cdot \vec{H} = 0, \tag{2.20}$$

$$\vec{\nabla} \times \vec{E} = i\omega\mu\vec{H}, \tag{2.21}$$

and

$$\vec{\nabla} \times \vec{H} = -i\omega\varepsilon\vec{E}, \tag{2.22}$$

at all interior points where ε and μ are continuous. Taking the curl of both sides of equations (2.21) and (2.22) leads to the vector wave equations

$$\nabla^2\vec{E} + k^2\vec{E} = 0 \tag{2.23}$$

and

$$\nabla^2\vec{H} + k^2\vec{H} = 0, \tag{2.24}$$

where

$$k^2 = \omega^2\varepsilon\mu. \tag{2.25}$$

Therefore, the fields must satisfy the vector wave equations.

2.4 Particles Small Compared to the Wavelength of Light

The absorption and scattering efficiencies of a spherical particle in an electric field with a wavelength much greater than the diameter of the particle are[14]

$$Q_{abs} = 4x\,\mathrm{Im}\left(\frac{\varepsilon_1 - \varepsilon_m}{\varepsilon_1 + 2\varepsilon_m}\right) \tag{2.26}$$

and

$$Q_{sca} = \frac{8}{3}x^4\left|\frac{\varepsilon_1 - \varepsilon_m}{\varepsilon_1 + 2\varepsilon_m}\right|^2, \tag{2.27}$$

where ε_1 and ε_m are the dielectric constants of the sphere and the surrounding material, respectively. The term $(\varepsilon_1 - \varepsilon_m)/(\varepsilon_1 + 2\varepsilon_m)$ also appears in the case of a spherical particle in a uniform *static* electric field, and suggests that we can use an electrostatic approximation when the particle size is much less than the wavelength of light. Because we actually use a wavelength dependent dielectric function in this model, this is often referred to as a *quasistatic* approximation.

For the case of a homogeneous, isotropic sphere embedded in an arbitrary medium, both of which are within a uniform static electric field,

$$\vec{E}_0 = E_0\hat{e}_z, \tag{2.28}$$

the initially uniform field will be distorted by an induced charge on the surface of the sphere due to the difference in dielectric constants of the sphere and host medium. The electric fields inside and outside the sphere, $\vec{E}_1$ and $\vec{E}_2$, respectively, are derivable from scalar potentials $\Phi_1(r,\theta)$ and $\Phi_2(r,\theta)$[14],

$$\vec{E}_1 = -\vec{\nabla}\Phi_1 \tag{2.29}$$

and

$$\vec{E}_2 = -\vec{\nabla}\Phi_2 ,$$

where

$$\nabla^2\Phi_1 = 0 \tag{2.30}$$

if $r < a$, and

$$\nabla^2\Phi_2 = 0 \tag{2.31}$$

if $r > a$, where a is the radius of the sphere. The potentials are independent of the azimuthal angle ϕ due to the spherical symmetry of the problem. The boundary conditions for the interface between the sphere and the medium are

$$\Phi_1 = \Phi_2 \tag{2.32}$$

and

$$\varepsilon_1 \frac{\partial\Phi_1}{\partial r} = \varepsilon_m \frac{\partial\Phi_2}{\partial r} , \tag{2.33}$$

for $r = a$. Additionally, at large distances from the sphere, the field is the unperturbed incident electric field

$$\lim_{r\to\infty}\Phi_2 = -E_0 r\cos\theta = -E_0 z . \tag{2.34}$$

It can be shown that the functions[14]

$$\Phi_1 = -\frac{3\varepsilon_m}{\varepsilon_1 + 2\varepsilon_m} E_0 r\cos\theta \tag{2.35}$$

and

$$\Phi_2 = -E_0 r\cos\theta + a^3 E_0 \frac{\varepsilon_1 - \varepsilon_m}{\varepsilon_1 + 2\varepsilon_m}\frac{\cos\theta}{r^2} \tag{2.36}$$

satisfy equations 2.19-2.24.

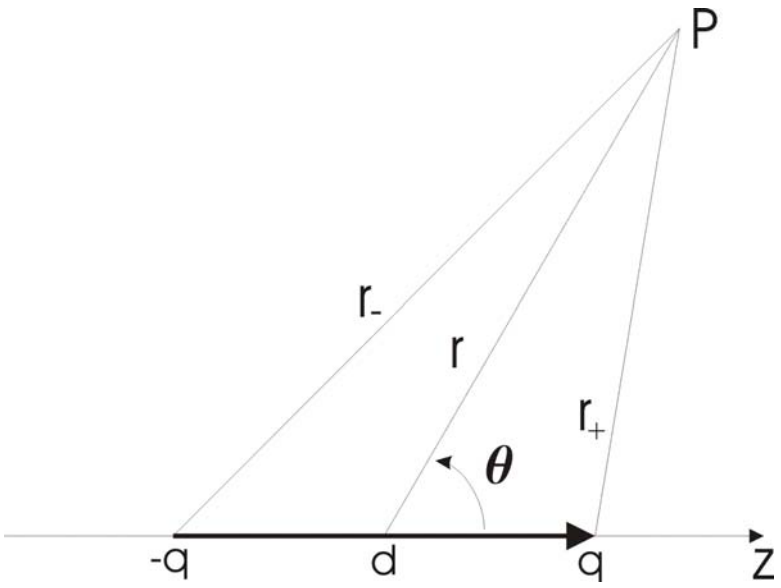

Figure 2.4-1: Electric dipole represented by a positive and negative charge q spaced a distance d from each other.[14]

If one looks at two point charges q and $-q$ separated by a distance d as in figure 2.4-1, the dipole moment is

$$\vec{p} = p\hat{e}_z , \tag{2.37}$$

where $\vec{p} = q\vec{d}$. The potential of the dipole embedded in a medium with dielectric constant ε_m at point P is

$$\Phi = \frac{q}{4\pi\varepsilon_m}\left(\frac{1}{r_+} - \frac{1}{r_-}\right), \tag{2.38}$$

where

$$r_+ = r\left(1 - \frac{\bar{r}\cdot\hat{e}_z}{r^2}d + \frac{d^2}{4r^2}\right)^{\frac{1}{2}} \tag{2.39}$$

and

$$r_{-} = r\left(1 + \frac{\vec{r}\cdot\hat{e}_z}{r^2}d + \frac{d^2}{4r^2}\right)^{\frac{1}{2}}. \tag{2.40}$$

If d is made to approach zero in such a way that qd remains constant, the ideal dipole potential is obtained

$$\Phi = \frac{\vec{p}\cdot\vec{r}}{4\pi\varepsilon_m r^3} = \frac{p\cos\theta}{4\pi\varepsilon_m r^2}. \tag{2.41}$$

When this is compared to equation (2.36), we can see that the potential outside of the spherical particle is the superposition of the incident field and the field from an ideal dipole at the origin with dipole moment

$$\vec{p} = 4\pi\varepsilon_m a^3 \frac{\varepsilon_1 - \varepsilon_m}{\varepsilon_1 + 2\varepsilon_m}\vec{E}_0, \tag{2.42}$$

or

$$\vec{p} = \varepsilon_m \alpha \vec{E}_0, \tag{2.43}$$

where α is the polarizability defined by the Claussius-Mossoti equation[15]

$$\alpha_i = 4\pi a^3 \frac{\varepsilon_i - \varepsilon_m}{\varepsilon_i + 2\varepsilon_m}. \tag{2.44}$$

This is the basic form of the polarizability that will be used in the next section.

2.5 Coupled-Dipole Model (CDM) for Nanocomposite Materials

The nanoparticle composite materials investigated in this research consist of large numbers of particles. In this section, the model will be constructed for a material in the absence of a magnetic field and, therefore, with constituents that do not posses off-diagonal components in their dielectric function. The basis for this approximation is that the individual particles can be represented as radiating electric dipoles. Each dipole radiates an electric dipole field as[16]

$$\vec{E} = \frac{1}{4\pi\varepsilon_0}\left\{\kappa^2\left(\hat{r}\times\vec{p}\right)\times\hat{r}\frac{e^{i\kappa r}}{r} + \left[3\hat{r}\left(\hat{r}\cdot\vec{p}\right) - \vec{p}\right]\left(\frac{1}{r^3} - \frac{i\kappa}{r^2}\right)e^{i\kappa r}\right\}. \tag{2.45}$$

The dipole, $\vec{p}$, is polarized in response to the incident field plus the fields radiated by all the other dipoles in the system. In this way, the Coupled-Dipole Model allows for an investigation of the near-field interactions between particles.

As a first approximation, each particle in the composite is replaced by a point dipole located at the point $\vec{r}_j$ with a scalar polarizability α_j. The polarization of each dipole is given by

$$\vec{P}_j = \alpha_j \vec{E}_j, \tag{2.46}$$

where $\vec{E}_j$ is the local electric field at point $\vec{r}_j$. When exposed to light, the electric field $\vec{E}_j$ is the sum of the incident field and the field emitted by all neighboring dipoles[17]

$$\vec{E}_{dipole,j} = -\sum_{k\neq j}\tilde{A}_{jk}\vec{P}_k, \tag{2.47}$$

where

$$\tilde{A}_{jk} = \frac{e^{i\kappa r_{jk}}}{r_{jk}}[\kappa^2(\hat{r}_{jk}\hat{r}_{jk} - \tilde{1}_3) + \frac{i\kappa r_{jk} - 1}{r_{jk}^{\ 2}}(3\hat{r}_{jk}\hat{r}_{jk} - \tilde{1}_3)], \tag{2.48}$$

and r_{jk} is the distance from particle j to particle k, and $\hat{r}_{jk}$ is the unit vector in the $\vec{r}_{jk}$ direction, with $\kappa = \omega / c$. The 3×3 identity matrix is represented by $\tilde{1}_3$. With some persistence, equation (2.47) can be shown to be analogous to equation (2.45). For *N* particles, the polarizations of each particle $\vec{P}_j$ can then by determined by solving the self-consistent system of 3*N* complex linear equations

$$\vec{E}_j + \sum_{k=1}^{N}\tilde{A}_{jk}\vec{P}_k = \vec{E}_{inc,j}, \tag{2.49}$$

where $\tilde{A}_{jj} = 0$, or, more compactly,

$$\sum_{k=1}^{N} \tilde{A}_{jk} \vec{P}_k = \vec{E}_{inc,j}, \tag{2.50}$$

where $\tilde{A}_{jj} = \alpha_j^{-1}$.

2.6 CDM in a Right-Left Circular Coordinate System

For the case where a magnetic field is applied, off-diagonal components of the dielectric tensor are non-zero. The tensor must be diagonalized as in equation (2.13) in order to use the Claussius-Mossoti equation to determine the polarizability. This is often done for particles that exhibit shape-dependent anisotropy[10] and the additional assumption is taken that the equation can be used for any diagonalized anisotropy. An identical transformation of the matrix $\tilde{A}_{jk}$ and the vectors $\vec{P}_k$ and $\vec{E}_{inc,j}$ is made which yields

$$\sum_{k=1}^{N} \tilde{A}_{jk}^{rl} \vec{P}_k^{rl} = \vec{E}_{inc,j}^{rl}, \tag{2.51}$$

with $\tilde{A}_{jj}^{rl} = \left(\tilde{\alpha}_j^{rl}\right)^{-1}$. Similarly, this allows for calculations of the polarizations of each particle.

2.7 Calculation of the Faraday Rotation

Solving Eq. (2.51) for the polarizations $\vec{P}_k^{rl}$, an average polarizability is determined from a volume average of the calculated polarizations

$$\bar{\bar{P}}^{rl} = \frac{1}{N} \sum_{k=1}^{N} \bar{P}_k^{rl}, \tag{2.52}$$

Effective dielectric components were found by using the inverse of the Classius-Mossotti relation

$$\bar{\varepsilon}_{ii} = \varepsilon_m \frac{a^3 + 2\bar{\alpha}_{ii}}{a^3 - \bar{\alpha}_{ii}}, \tag{2.53}$$

using the averaged polarizability. The Faraday rotation spectrum can then be calculated from[9]

$$\theta = \mathrm{Re}\left[\frac{\pi}{\lambda}\frac{\bar{\varepsilon}_{xy}}{\sqrt{\bar{\varepsilon}_{xx}}}\right], \tag{2.54}$$

where $\bar{\varepsilon}_{xx}$ and $\bar{\varepsilon}_{xy}$ are the effective diagonal and off-diagonal components in Cartesian coordinates, respectively. Alternatively, the ellipticity can be determined by taking the imaginary part of equation (2.54).

CHAPTER 3: EXPERIMENT

3.1 Experimental Setup for Magneto-Optic Measurements

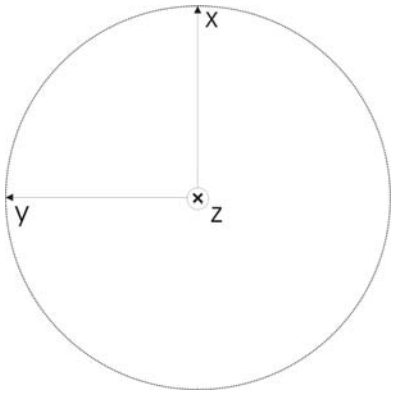

Figure 3.1-1: Coordinate system for the experimental setup looking towards the light source, which propagates down the z-axis.

The experimental setup shown in figure 3.1-2 was used for the measurement of Faraday rotation and ellipticity as a function of wavelength. A broadband light source is fed through a monochromator which gives a spectral range from approximately 400 to 1000 nanometers. The "unpolarized" light then passes through a linear polarizer set at 45 degrees from the x-axis before it is sent through a photoelastic modulator (PEM). The PEM causes the light to undergo a periodically changing polarization from right-handed circular (RHCP) to left-handed circular (LHCP). The modulated light then passes through holes bored through the axis of a 2 Tesla electromagnet. A sample is placed between the poles of the magnet. Next, the light passes

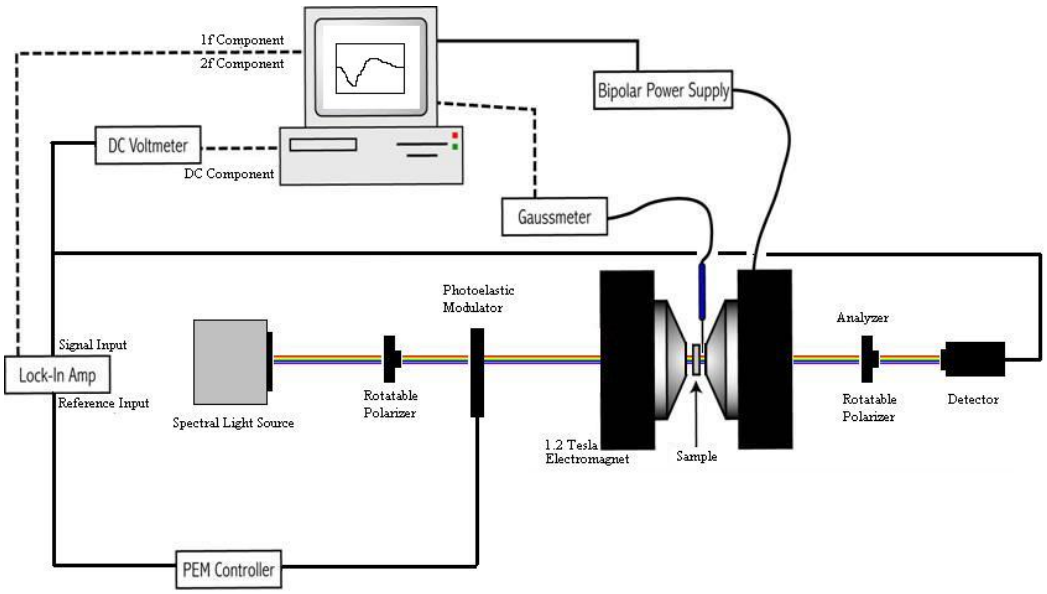

Figure 3.1-2: Experimental setup for magneto-optical measurements.

through an analyzer, which is another linear polarizer set parallel to the x-axis. At the end of the light path, the signal is detected by a silicon photodiode.

3.2 PEM Method of Polarization measurement

The photoelastic modulator is essentially a periodically varying quarter wave plate made from a fused silica optical element. The fused silica element is attached to a piezoelectric transducer, which induces mechanical strain along one if its axis. The strain causes a birefringence proportional to the resulting stress, otherwise known as the photoelastic effect. Because the light passes through the element at 45^{o} and the strain of the PEM is along the y-axis of the optical system, the phase of the y-component of the linearly polarized incident light is periodically lagged. This is what causes the light to periodically shift between RHCP and LHCP (fig. 3.2-1).

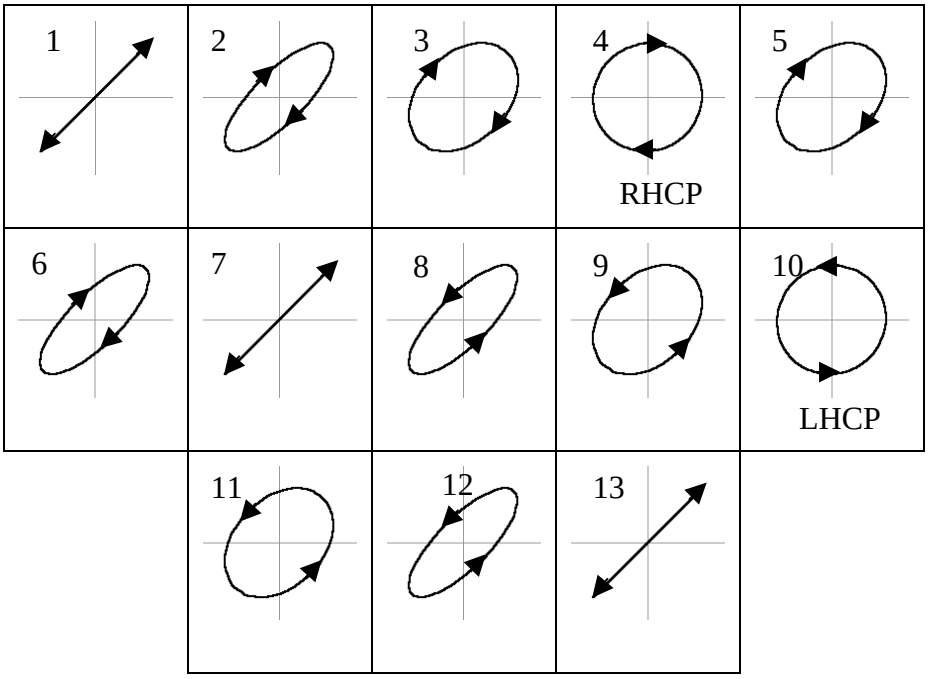

Figure 3.2-1: Modulation of linearly polarized light as it passes through the photoelastic modulator at 45^o.[18]

With the above mentioned optically elements and periodically varying polarization of the incident light, it can be shown through Jones matrix calculations that the Faraday rotation and ellipticity is proportional to the normalized second and first harmonic, respectively.[18] That is

$$\theta = A\frac{I_{2f}}{I_{DC}}, \tag{53}$$

and

$$\eta = B\frac{I_{1f}}{I_{DC}}, \tag{54}$$

where I_{2f} is the 2f signal, I_{1f} is the 1f signal, I_{DC} is the DC signal, and A and B are calibration constants determined by the optical system.

3.3 Sample Preparation

Samples were prepared by combining varying amounts of a magnetite nanoparticle solution with a 10% solution of poly(methylmethacrylate) PMMA and toluene (fig. 3.3-1). Magnetite nanoparticles (fig. 3.3-2) were synthesized using the method of Caruntu, et al.[19] Briefly, $FeCl_3$ and $FeCl_2$ were dissolved in diethylene glycol yielding a solution containing Fe^{3+} and Fe^{2+} ions in the ratio of 2:1. Coprecipitation with NaOH at ~200^{o}C resulted in 8-10 nm Fe_3O_4 particles. The nanoparticles were washed, dried and suspended in toluene by the addition of oleic acid as a capping ligand. The concentration of this solution was approximately 5 mg/ml. Volume fractions of 3-25 percent nanoparticles were prepared, which corresponded to interparticle distances of approximately 10-20 nanometers. Thin films were prepared by spin-coating 20 ml of the solution onto quartz disks for 9 minutes at 150 RPM.

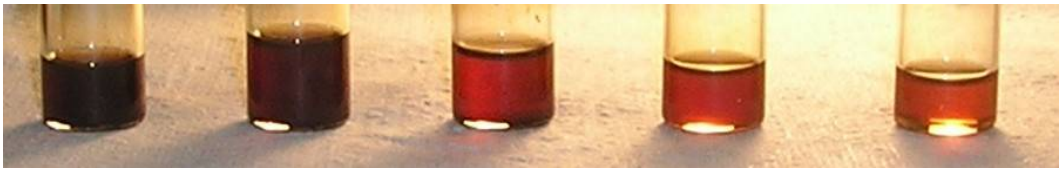

Figure 3.3-1: Vials containing different concen-trations of magnetite nanoparticles.

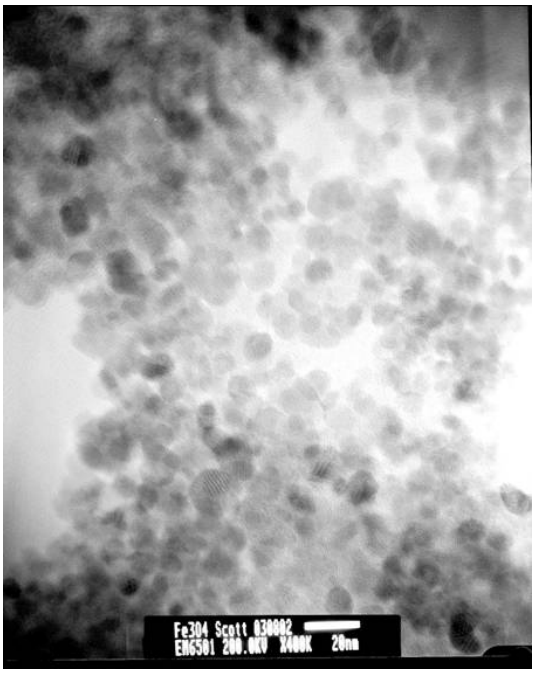

Figure 3.3-2: TEM image of magnetite nano-particles.

CHAPTER 4: RESULTS

4.1 Experimental Results

Figure 4.1-1 shows the experimental Faraday rotation spectra of magnetite nanoparticle/PMMA composite films. By increasing the concentration of magnetite in the composite materials, shifts in the main spectral feature of the Faraday rotations by up to approximately 92 nm are observed. Films produced with dilute concentrations of nanoparticles exhibited peaks at approximately 470 nm, while those at higher concentrations shifted towards red wavelengths. The largest shift was observed for the two most concentrated composites at approximately 560 nm. Typically, magneto-optic materials are modeled using effective medium

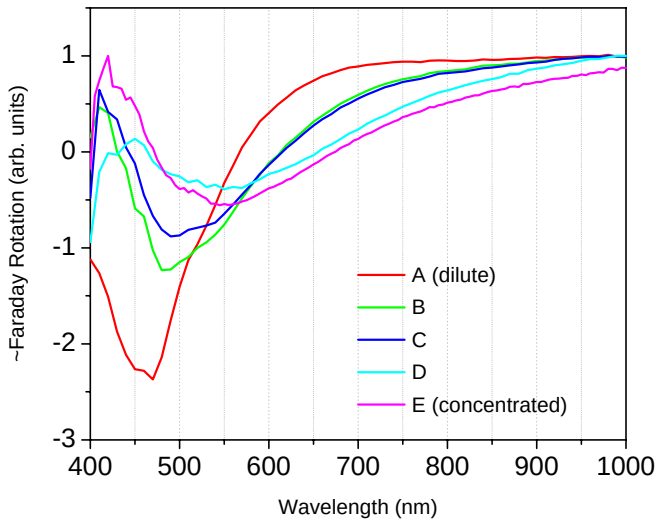

Figure 4.1-1: Experimental Faraday rotation spectra for various nanoparticle concentrations.

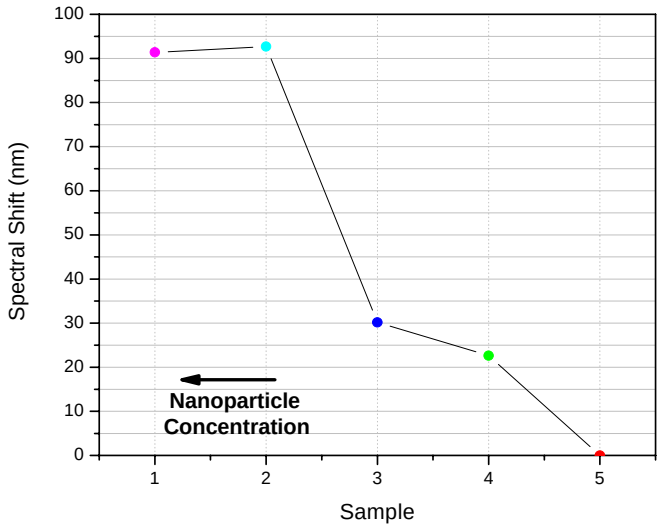

Figure 4.1-2: Spectral shift of experimental data for various concentrations of nanoparticles.

theory (EMT).[9] These shifts in the spectral peak are not predicted by EMT, which does not account for optical interactions between the particles.

4.2 Calculations of Two-Particle Geometries

We use our coupled-dipole model to explicitly account for particle-particle interactions. First, we limit the calculations to two coupled Fe_3O_4 nanoparticles of 8 nm diameter and find that this is sufficient to reproduce the qualitative features of the measured Faraday rotation spectrum. We calculate the spectrum for the three basic orthogonal two-particle geometries shown in figures 4.2-1 to 4.2-3. In these calculations, the magnetic field is parallel to the direction of light propagation, taken to be the *z*-direction, consistent with equation (2.10). The polarization of the incident light is linear in the *x*-direction for all calculations. We used literature values for diagonal components of the dielectric tensor of Fe_3O_4 in Eq. (2.10) taken from data reported by

Schlegel, et al.[20] and off-diagonal components taken from Zhang, et al.[21] A dielectric constant of 1.49 was used for the PMMA (ε_{hst}). These values can be found in Appendix A.

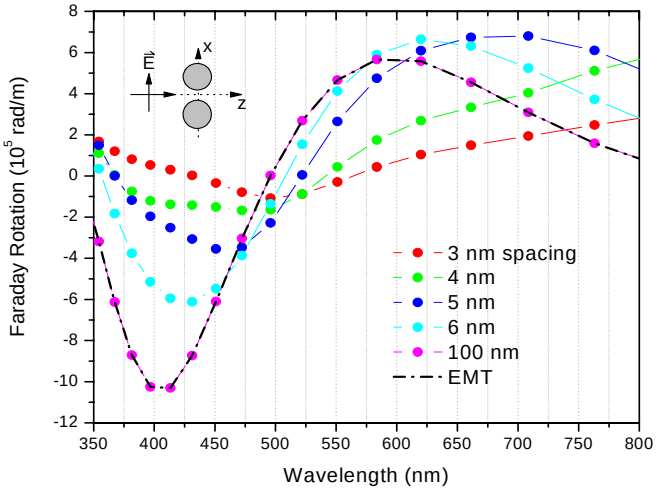

Figure 4.2-1: Calculation of the Faraday rotation spectra for two nanoparticles with various interparticle distances. Geometry is indicated in the inset.

For all three two-particle geometries, little change was seen in the spectra until the particles were brought within approximately 6 nm of each other. In fact, for interparticle distances greater than 6 nm, our calculation is similar to EMT, which is included in the figures for comparison. Figure 4.2-1 shows the theoretical results for two particles aligned on the *x*-axis, perpendicular to the propagation direction and parallel to the linear polarized light. This geometry shows a progressive red-shift of approximately 92 nm for dipoles with a 3 nm spacing. In figure 4.2-2,

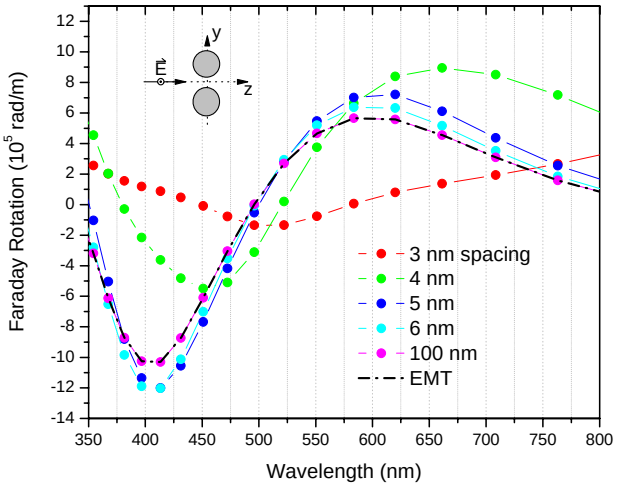

Figure 4.2-2: Calculation of the Faraday rotation spectra for two nanoparticles with various interparticle distances. Geometry is indicated in the inset.

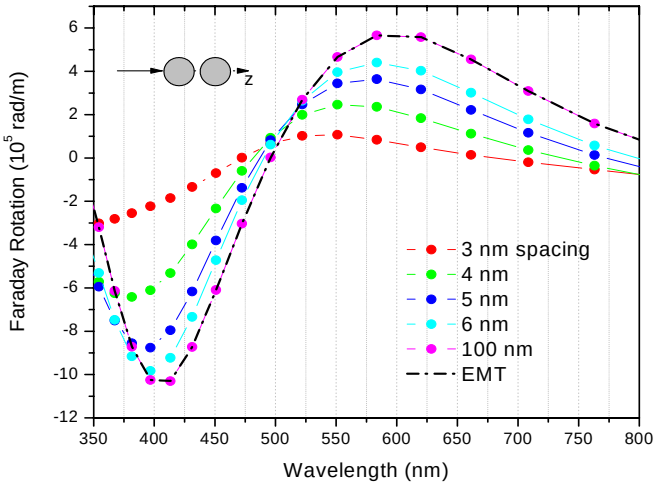

Figure 4.2-3: Calculation of the Faraday rotation spectra for two nanoparticles with various interparticle distances. Geometry is indicated in the inset.

the particles are, again, aligned perpendicular to the propagation direction, but with the incident light polarized perpendicular to the particles. Red-shifts are shown with a maximum of around 105 nm, but no significant shift is seen in the spectra until the particles are within 4 nm. In the last two-particle geometry, shown in figure 4.2-3, the particles are aligned parallel to the propagation direction. In contrast to the other geometries, blue-shifting is observed in these calculations by approximately 97 nm at a 3 nm spacing. We point out that if we assume we have

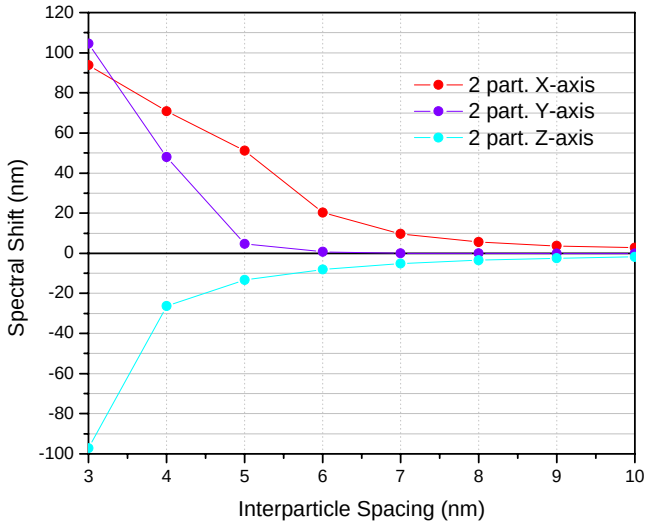

Figure 4.2-4: Summary of the spectral shifts of each two-particle geometry.

8-nm diameter particles, separations less than 8 nm would correspond to particles that physically overlap. This is justified within this approximation since the physical particle is replaced by a radiating *point* dipole at the particle's position. Size is only taken into account in calculating the "strength" of the polarizability equation 2.44. Phenomenologically, this overlap has been suggested to account for multipolar corrections to the depolarization factor. A summary of the spectral shifts of the three geometries is provided in figure 4.2-4.

4.3 Cubic Arrays of Particles

In the experimental system, the particles are expected to be randomly distributed with an average interparticle spacing determined by the volume fraction of nanoparticles to PMMA host material. The measured spectrum would then be an average of the three basic particle geometries of figures 4.2-1 through 4.2-3. The Faraday spectra of three cubic arrays of particles were calculated in order to confirm that a net red-shift would occur from a combination of the three two-particle geometries. In addition, by calculating an increasing number of nanoparticle cubic arrays, an estimate of the amount of neighboring particles contributing to the spectral shift was able to be determined. The Faraday spectra of the cubic arrays confirm a net red-shift as the interparticle spacing is decreased. The largest red-shift of approximately 123 nm is shown for the 6x6x6 cubic array (fig 2.3-3). As the number of particles in the model is increased, the red-shift appears to converge at the 120-130 nm range. This suggests that the system of approximately 216 particles is sufficient to account for contributions from neighboring particles.

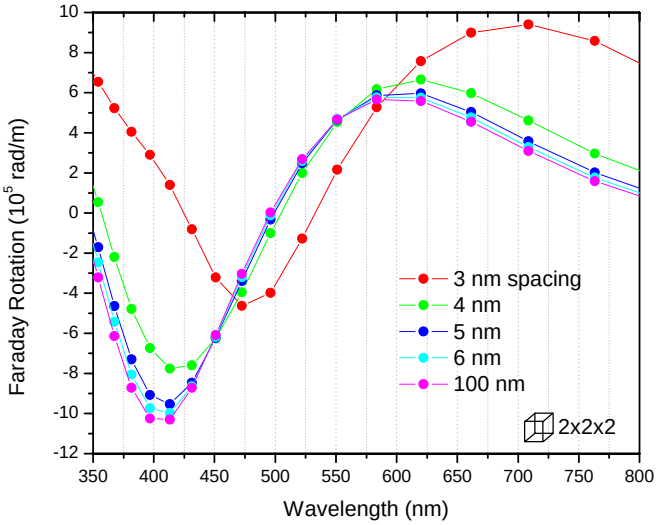

Figure 4.3-1: Calculation of the Faraday spectra for a 2x2x2 cubic array of nanoparticles with various spacings.

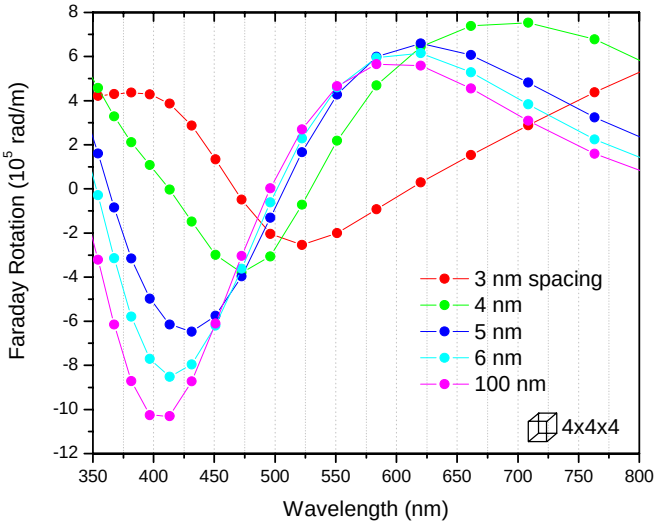

Figure 4.3-2: Calculation of the Faraday spectra for a 4x4x4 cubic array of nanoparticles with various spacings.

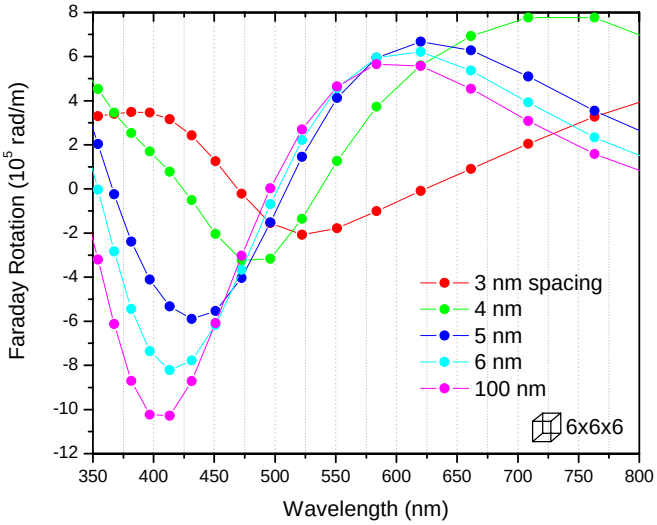

Figure 4.3-3: Calculation of the Faraday spectra for a 6x6x6 cubic array of nanoparticles with various spacings.

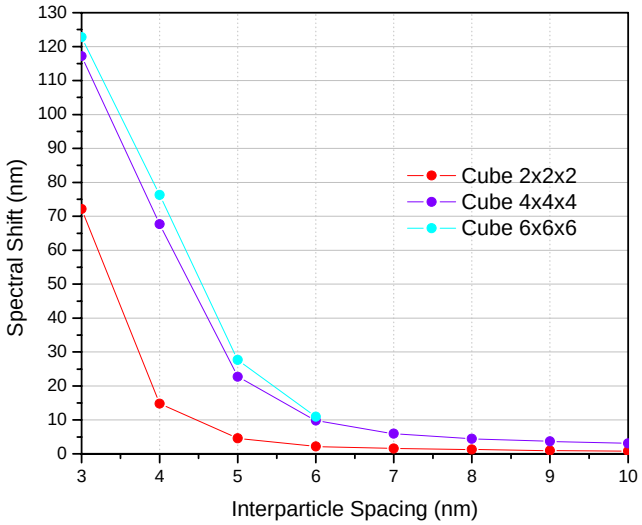

Figure 4.3-4: Summary of the spectral shift for three cubic arrays of nanoparticles.

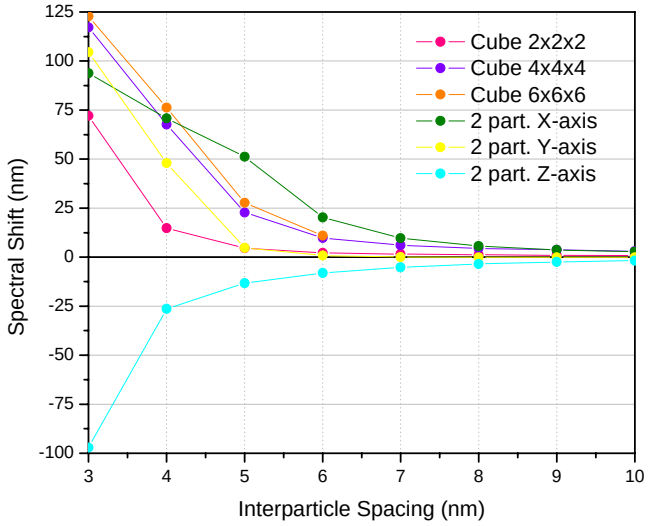

Figure 4.3-5: Summary of the spectral shift for two-particle and cubic geometries.

CHAPTER 5: CONCLUSION

Peak position of the Faraday rotation spectrum of magnetite/PMMA nanocomposite films is shown to be concentration dependent. By increasing the concentration of 8 nm diameter particles in the PMMA matrix, a red-shift and broadening of the main spectral feature is observed. Calculations using existing EMT models fail to account for the shifts seen in the experimental data. Using a coupled-dipole-based model, shifts in peak position are shown to occur based purely on optical effects where only the inter-particle distance is varied. In addition, the peak positions of the calculated spectra depend on the geometrical configuration. It is also shown that the main features of the Faraday spectra can be calculated by taking into account nearest neighbor effects. Models of cubic arrays show a net red-shifting of the peak position as the concentration of particles is increased.

Future directions for this research might include improved characterization of the distribution of nanoparticles in the material. This would allow for a better choice of particle arrangement within the model. Additionally, particles might be better approximated by a discrete-dipole model, where individual particles are made up of large amounts of dipoles. Along these lines, more complex structures could be obtained, such as cylinders and rough surfaces.

REFERENCES

[1] S. A. Maier, M. L. Brongersma, P. G. Kik, S. Meltzer, A. A. G. Requicha, and H. A. Atwater, Adv. Mater. 13, 1501-1505 (2001).

[2] L. A. Kelly, E. Coronado, L. L. Zhao, and G. C. Schatz, JPCB 107, 668-677 (2003).

[3] M. L. Brongersma, J. W. Hartman, and H. A. Atwater, PRB 62, R16356-R16359 (2000).

[4] A. Yasumori, H. Matsumoto, S. Hayashi, and K. Okada, J. Sol-Gel Sci. Technol. 18, 249 (2000).

[5] H. W. Davies and J. P. Llewllyn, J. Phys. D: Appl. Phys 13, 2327-2336 (1980).

[6] Y. A. Barnakov, B. L. Scott, V. Golub, L. Kelly, V. Reddy, and K. L. Stokes, J. Phys. Chem. Solids 65, 1005 (2004).

[7] Z. Q. Qiu and S. D. Bader, Rev. of Sci. Instr. 71, 1243 (2000).

[8] A. Zvezdin and V. Kotov, *Modern Magnetooptics and Magnetooptical Materials* (Inst. of Phys. Pub., 1997).

[9] M. Abe and M. Gomi, Japan. J. Appl. Phys. 23, 1580 (1984).

[10] B. T. Draine, Astophys. J. 333, 848 (1988).

[11] A. A. Lazarides and G. C. Schatz, J. Phys. Chem. B 104, 460-467 (2000).

[12] R. M. A. Azzam and N. M. Bashara, *Ellipsometry and Polarized Light* (Elsevier Science Pub Co, 1999).

[13] S. Wittekoek, T. J. A. Pompa, J. M. Robertson, and P. F. Bongers, Phys. Rev. B 12, 2777-2788 (1975).

[14] C. F. Bohren and D. R. Huffman, *Absorption and Scattering of Light by Small Particles* (John Wiley & Sons, Inc., 1983).

[15] K. Urano and M. Inoue, J. Chem. Phys. 66, 791 (1977).

[16] J. D. Jackson, *Classical Electrodynamics* (John Wiley & Sons, Inc., 1998).

[17] B. T. Draine and P. J. Flatau, J. Opt. Soc. Am. A 11, 1491 (1994).

[18] S. Dennis, Thesis, University of New Orleans, 2001.

[19] D. Caruntu, Y. Remond, N. H. Chou, M.-J. Jun, G. Caruntu, J. He, G. Goloverda, C. O'Connor, and V. Kolesnichenko, Inorg. Chem. 41, 6137 (2002).

[20] A. Schlegel, S. F. Alvarado, and P. Wachter, J. Phys. C: Solid State Phys. 12, 1157 (1978).

[21] X. Zhang, J. Schoenes, and P. Wachter, Solid State Commun. 39, 189 (1981).

Appendix A: Dielectric Constants

Energy (eV)	Re[ε_{xx}]	Im[ε_{xx}]
1.500	5.000	2.000
1.625	5.229	2.171
1.750	5.235	2.465
1.875	5.125	2.774
2.000	5.000	3.000
2.125	4.940	3.069
2.250	4.940	3.054
2.375	4.969	3.065
2.500	5.000	3.200
2.625	5.003	3.536
2.750	4.966	3.979
2.875	4.869	4.410
3.000	4.700	4.700
3.125	4.454	4.761
3.250	4.160	4.645
3.375	3.859	4.444
3.500	3.600	4.250
3.625	3.404	4.129
3.750	3.272	4.081
3.875	3.174	4.079
4.000	3.100	4.100

Table B-1: Real and imaginary parts of the diagonal dielectric tensor elements for magnetite.

Energy (eV)	Re[ε_{xy}]	Im[ε_{xy}]
1.500	0.042	0.010
1.625	0.035	0.016
1.750	0.025	0.023
1.875	0.015	0.028
2.000	0.005	0.029
2.125	-0.005	0.025
2.250	-0.012	0.017
2.375	-0.016	0.007
2.500	-0.014	-0.004
2.625	-0.005	-0.014
2.750	0.007	-0.021
2.875	0.021	-0.025
3.000	0.031	-0.025
3.125	0.036	-0.020
3.250	0.037	-0.013
3.375	0.034	-0.003
3.500	0.031	0.005
3.625	0.028	0.011
3.750	0.025	0.016
3.875	0.023	0.019
4.000	0.021	0.022

Table B-2: Real and imaginary parts of the off-diagonal dielectric tensor elements for magnetite.

APPENDIX B: MATHEMATICA PROGRAM FOR TWO-PARTICLE CALCULATIONS

```
(* Program for calculation of extinction and Magneto-
  Optic Spetra of two particles *)

(* Turn Off Spell Checker *)
Off[General::spell]

(* Import Dielectric Constants (each file must contain the same amount of entries)*)
perm1d = Import["D:\permittivity\Fe3O4-diagonal2.txt", "Table"];
perm1o = Import["D:\permittivity\Fe3O4-offdiagonal2.txt", "Table"];

(* Number of Entries For Energy/Dielectric Constants *)
num = Length[perm1d];

(* Extract Dielectric Info *)
xx1 = Table[(perm1d[[i]])[[2]] + I (perm1d[[i]])[[3]], {i, num}];
xy1 = Table[(perm1o[[i]])[[2]] + I (perm1o[[i]])[[3]], {i, num}];
enr = Table[(perm1d[[i]])[[1]], {i, num}];

(* Host dielectric constant, particle radius, and inter-particle distance *)
host = (1.49)^2;
size = 4 ;
d = 3 // N;

(* Transformation Matrices *)
finv = 1/Sqrt[2] {{1, I, 0}, {1, -I, 0}, {0, 0, Sqrt[2]}};
f = 1/Sqrt[2] {{1, 1, 0}, {-I, I, 0}, {0, 0, Sqrt[2]}};

(* Unit Vectors "Cartesian" *)
r12 = {-1, 0, 0};
r21 = {1, 0, 0};

(* Incident Wave at Dipole 1 and 2 "Cartesian" *)
ei = {1, 0, 0};

(* Incident Wave "Right/Left" *)
eirl = finv . ei;

(* The "TOTAL" Electric Field at Dipole 1 and 2 "Cartesian" *)
e1 = {e1x, e1y, e1z};
e2 = {e2x, e2y, e2z};

(* The "TOTAL" Electric Field at Dipole 1 and 2 "Right/Left" *)
e1rl = finv . e1;
e2rl = finv . e2;

(* Identity Matrix *)
im = {{1, 0, 0}, {0, 1, 0}, {0, 0, 1}};
```

```
(* Dummy Arrays *)
cextl = {};
effeps = {};

(* Loop For Calculating C_ext Spectrum *)
Do[
  (* Dielectric Functions "Cartesian" *)
  ϵ1 = {{xx1[[n]], I xy1[[n]], 0}, {-I xy1[[n]], xx1[[n]], 0}, {0, 0, xx1[[n]]}};

  ϵ2 = {{xx1[[n]], I xy1[[n]], 0}, {-I xy1[[n]], xx1[[n]], 0}, {0, 0, xx1[[n]]}};

  (* Conversian of Dielectric Functions to Right/Left Circular *)
  ϵ1rl = finv . ϵ1 . f;
  ϵ2rl = finv . ϵ2 . f;

  (* Polarizability *)
  alp1 = size^3 {{(ϵ1rl[[1]])[[1]] - host / ((ϵ1rl[[1]])[[1]] + 2 host), 0, 0},
     {0, (ϵ1rl[[2]])[[2]] - host / ((ϵ1rl[[2]])[[2]] + 2 host), 0}, {0, 0, (ϵ1rl[[3]])[[3]] - host / ((ϵ1rl[[3]])[[3]] + 2 host)}};
  alp2 = size^3 {{(ϵ2rl[[1]])[[1]] - host / ((ϵ2rl[[1]])[[1]] + 2 host), 0, 0}, {0, (ϵ2rl[[2]])[[2]] - host / ((ϵ2rl[[2]])[[2]] + 2 host), 0},
     {0, 0, (ϵ2rl[[3]])[[3]] - host / ((ϵ2rl[[3]])[[3]] + 2 host)}};

  (* Wavelength *)
  λ = 1242 / enr[[n]];

  (* Wave Number *)
  k = 2 π / λ Sqrt[host];

  (* Polarization *)
  p1 = alp1 . e1rl;
  p2 = alp2 . e2rl;

  (* Individual "a" Matrices "Cartesian" *)
  a12 = (E^(I k d) / d) (k^2 (Outer[Times, r12, r12] - im) + (I k d - 1) / d^2 (3 Outer[Times, r12, r12] - im));
  a21 = (E^(I k d) / d) (k^2 (Outer[Times, r21, r21] - im) + (I k d - 1) / d^2 (3 Outer[Times, r21, r21] - im));

  (* Individual "a" Matrices "Right/Left" *)
  a12rl = finv . a12 . f;
  a21rl = finv . a21 . f;

  (* Create Total 3 n x 3 n "A" Matrix *)
  a = Table[0, {6}, {6}];
  Do[a = ReplacePart[a, Join[a12rl[[i]], {0, 0, 0}], i], {i, 3}];
```

```
Do[a = ReplacePart[a, Join[{0, 0, 0}, a21rl[[i]]], i + 3], {i, 3}];

(* Create 1 x 6 Polarization Matrix *)
p = Join[p2, p1];

(* Electric Field Contribution from Neighboring Paricle *)
ap = a.p;

(* Total Electric Field From All Contributions *)
ed = Join[e1rl, e2rl];

(* Total Electric Field at Particle + Contribution *)
edap = ed + ap;

(* Incident Linear Polarized Light "Right/Left" *)
eit = Join[eirl, eirl];

(* Solve for electric field *)
sol1 = Solve[{edap[[1]] == eit[[1]], edap[[2]] == eit[[2]],
   edap[[3]] == eit[[3]], edap[[4]] == eit[[4]], edap[[5]] == eit[[5]],
   edap[[6]] == eit[[6]]}, {e1x, e1y, e1z, e2x, e2y, e2z}];

e1xt = e1x /. sol1[[1]];
e1yt = e1y /. sol1[[1]];
e1zt = e1z /. sol1[[1]];
e2xt = e2x /. sol1[[1]];
e2yt = e2y /. sol1[[1]];
e2zt = e2z /. sol1[[1]];

(* Calculate polarizations *)
p1f = alp1.{(e1xt + I e1yt)/Sqrt[2], (e1xt - I e1yt)/Sqrt[2], e1zt};
p2f = alp2.{(e2xt + I e2yt)/Sqrt[2], (e2xt - I e2yt)/Sqrt[2], e2zt};

(* Convert Polarization Back to Cartesian *)
p1c = f . p1f;
p2c = f . p2f;

(* Formula for extinction spectra *)
cext[ei1_, ei2_, pol1_, pol2_] =
 4 π k (Im[Conjugate[ei1].pol1] + Im[Conjugate[ei2].pol2]);

(* Calculate extinction spectra and add to list *)
cextl = Append[cextl, {λ, cext[ei, ei, p1c, p2c]}];

(* Calculate effective polarization for the materials *)
effpol = Solve[{p1f[[1]] == αxx eirl[[1]], p1f[[2]] == αyy eirl[[1]]}, {αxx, αyy}];

(* Effective polarizability *)
```

```
  alpxx = αxx  /. effpol[[1]];
  alpyy = αyy  /. effpol[[1]];

  (* Effective dielectric constant *)
  effepsxx = (-2 alpxx host - size^3 host)/(alpxx - size^3);
  effepsyy = (-2 alpyy host - size^3 host)/(alpyy - size^3);

  (* Convert effective dielectric tensor to cartesian coordinates *)
  effepscon = f . {{effepsxx, 0, 0}, {0, effepsyy, 0}, {0, 0, 1}} . finv;

  (* Add converted dielectric tensor elements and wavelengths to list *)
  effeps = Append[effeps, {λ, (effepscon[[1]])[[1]], (effepscon[[2]])[[1]]}];

  , {n, num}];

(* Plot extinction spectrum *)
ListPlot[cextl, PlotJoined → True, PlotLabel → d "= d"]

(* Calculate Faraday rotation *)
rot =
  Table[{(effeps[[n]])[[1]], Re[π/(effeps[[n]])[[1]] (effeps[[n]])[[3]]/Sqrt[(effeps[[n]])[[2]]]]}, {n, num}];

(* Plot Faraday rotation *)
ListPlot[rot, PlotJoined → True, PlotRange → All, PlotLabel -> "nm = d" d]
```

APPENDIX C: MATLAB PROGRAM FOR ARBITRARY PARTICLE ARRANGEMENTS

```
function result=DArl(targetnum,parameter1,parameter2,parameter3,dipolespacing,...
    radius1,radius2,eps1diag,eps1off,eps2diag,eps2off,hstN,E_inc,plot)

% create target
target_1=DAtarget(targetnum,parameter1,parameter2,parameter3,dipolespacing);

% total number of dipoles on grid
[dim1,dim2,dim3]=size(target_1);
totaldipoles=dim1*dim2*dim3;

% host dielectric function
hsteps=hstN^2;

% transformation matrix
f=1/sqrt(2)*[1,1,0;-i,i,0;0,0,sqrt(2)];

% count the number of eps1 and eps2 dipoles
eps1dipoles=0;
eps2dipoles=0;
x=1;
y=1;
z=1;
while z<=dim3
    if target_1(x,y,z)==1
        eps1dipoles=eps1dipoles+1;
    end
    if target_1(x,y,z)==2
        eps2dipoles=eps2dipoles+1;
    end
    if x==dim1
        x=1;
        if y==dim2
            y=1;
            z=z+1;
        else
            y=y+1;
        end
    else
        x=x+1;
    end
end

% import dielectric constants
path='D:\permittivity\';
file1=[path,eps1diag,'.txt'];
file2=[path,eps1off,'.txt'];
file3=[path,eps2diag,'.txt'];
file4=[path,eps2off,'.txt'];
eps1diagtable=importdata(file1);
eps1offtable=importdata(file2);
eps2diagtable=importdata(file3);
```

```
eps2offtable=importdata(file4);
num=max(size(eps1diagtable));
for n=1:num
    nextlambda=1240/eps1diagtable(n,1);
    nexteps1diag=eps1diagtable(n,2)+i*eps1diagtable(n,3);
    nexteps1off=eps1offtable(n,2)+i*eps1offtable(n,3);
    nexteps2diag=eps2diagtable(n,2)+i*eps2diagtable(n,3);
    nexteps2off=eps2offtable(n,2)+i*eps2offtable(n,3);
    if n==1
        lambda=nextlambda;
        eps1diag=nexteps1diag;
        eps1off=nexteps1off;
        eps2diag=nexteps2diag;
        eps2off=nexteps2off;
    else
        lambda=[lambda;nextlambda];
        eps1diag=[eps1diag;nexteps1diag];
        eps1off=[eps1off;nexteps1off];
        eps2diag=[eps2diag;nexteps2diag];
        eps2off=[eps2off;nexteps2off];
    end
end


% compute faraday spectrum
for n=1:num
    eps1matrix=[eps1diag(n),i*eps1off(n),0;-i*eps1off(n),eps1diag(n),0;0,0,eps1diag(n↙
)];
    eps2matrix=[eps2diag(n),i*eps2off(n),0;-i*eps2off(n),eps2diag(n),0;0,0,eps2diag(n↙
)];
    k=2*pi/(lambda(n)/hstN);
    dipole_calc=DAcalc(f,k,eps1matrix,eps2matrix,radius1,radius2,hsteps,target_1,eps1↙
dipoles,...
        eps2dipoles,dim1,dim2,dim3,dipolespacing,E_inc,plot);
    if plot==1
        nextfaraday=(pi/lambda(n))*(dipole_calc(2)/sqrt(dipole_calc(1)));
        if n==1
            faraday=nextfaraday;
        else
            faraday=[faraday;nextfaraday];
        end
    else
        for j=1:totaldipoles
            nextsinext=4*pi*k*imag(conj(rot90(E_inc))*(f*[dipole_calc(1+3*(j-1));dipo↙
le_calc(2+3*(j-1));dipole_calc(3+3*(j-1))]));
            if j==1
                sinext=nextsinext;
            else
                sinext=sinext+nextsinext;
            end
        end
```

```
        if n==1
            ext=sinext;
        else
            ext=[ext;sinext];
        end
    end
end

% return faraday if plot==1 and ext if plot==2
if plot==1
    result=[lambda,real(faraday)];
else
    result=[lambda,ext];
end

save mydata.txt result -ascii -tabs

x=1;
y=1;
z=1;
c=1;
while z<=dim3
    if target_1(x,y,z)==1
        plot3(x,y,z,'bo','MarkerEdgeColor','k','MarkerFaceColor','k','MarkerSize',2)
    end
    if c==1
        hold on
    end
    if c==dim1*dim2*dim3
        hold off
    end
    c=c+1;
    if x==dim1
        x=1;
        if y==dim2
            y=1;
            z=z+1;
        else
            y=y+1;
        end
    else
        x=x+1;
    end
end
```

```
function result=DAcalc(f,k,eps1,eps2,radius1,radius2,hsteps,target_1,eps1dipoles,...
    eps2dipoles,dim1,dim2,dim3,dipolespacing,E_inc,plot)

% polarization
epsrl1=inv(f)*eps1*f;
epsrl2=inv(f)*eps2*f;
alpha1=radius1^3*[(epsrl1(1,1)-1*hsteps)/(epsrl1(1,1)+2*hsteps),0,0;0,(epsrl1(2,2)-1*hsteps)/(epsrl1(2,2)+2*hsteps),0;...
        0,0,(epsrl1(3,3)-1*hsteps)/(epsrl1(3,3)+2*hsteps)];
alpha2=radius2^3*[(epsrl2(1,1)-1*hsteps)/(epsrl2(1,1)+2*hsteps),0,0;0,(epsrl2(2,2)-1*hsteps)/(epsrl2(2,2)+2*hsteps),0;...
        0,0,(epsrl2(3,3)-1*hsteps)/(epsrl2(3,3)+2*hsteps)];

% initialize counters and create A matrix
xo=1;
yo=1;
zo=1;
x=1;
y=1;
z=1;
Ajk=[];
A=[];
while zo<=dim3
    while z<=dim3
        if target_1(xo,yo,zo)==0
            % Do nothing
        else
            if x==xo & y==yo & z==zo
                if target_1(x,y,z)==1
                    nextAjk=inv(alpha1);
                else
                    nextAjk=inv(alpha2);
                end
            else
                rjk=sqrt((x-xo)^2+(y-yo)^2+(z-zo)^2)*dipolespacing;
                rjkhatcol=([xo;yo;zo]-[x;y;z])/(rjk/dipolespacing);
                rjkhatrow=([xo,yo,zo]-[x,y,z])/(rjk/dipolespacing);
                nextAjk=inv(f)*((exp(i*k*rjk)/rjk)*(k^2*((rjkhatcol*rjkhatrow)-eye(3))+((i*k*rjk-1)/rjk^2)*...
                    (3*(rjkhatcol*rjkhatrow)-eye(3))))*f;
            end
        end

        if target_1(x,y,z)==0 | target_1(xo,yo,zo)==0
            % Do nothing
        else
            if length(Ajk)==0
                Ajk=nextAjk;
            else
                Ajk=[Ajk,nextAjk];
            end
```

```
        end

        if x==dim1
            x=1;
            if y==dim2
                y=1;
                z=z+1;
            else
                y=y+1;
            end
        else
            x=x+1;
        end
    end

    if target_1(xo,yo,zo)==0
        % Do nothing
    else
        if length(A)==0
            A=Ajk;
        else
            A=[A;Ajk];
        end
    end

    if xo==dim1
        xo=1;
        if yo==dim2
            yo=1;
            zo=zo+1;
        else
            yo=yo+1;
        end
    else
        xo=xo+1;
    end
x=1;
y=1;
z=1;
Ajk=[];
end

% create incident electric field vector
Eincrl=inv(f)*E_inc;
for n=1:length(A)/3
    next=Eincrl;
    if n==1
        Einc=next;
    else
        Einc=[Einc;next];
    end
```

```
end

% Solve for the dipole polarizations
P=lsqr(A,Einc,1e-5,100000);

% Average polarization
for n=1:length(A)/3
    nextP1=P(1+3*(n-1));
    nextP2=P(2+3*(n-1));
    if n==1
        P1=nextP1;
        P2=nextP2;
    else
        P1=P1+nextP1;
        P2=P2+nextP2;
    end
end
P1avg=P1/(eps1dipoles+eps2dipoles);
P2avg=P2/(eps1dipoles+eps2dipoles);

% average dielectric constant
alphaeffxx=P1avg/Eincrl(1);
alphaeffyy=P2avg/Eincrl(2);
averageradius=(eps2dipoles*radius2+eps1dipoles*radius1)/(eps1dipoles+eps2dipoles);
epseffxx=(hsteps*(averageradius^3+2*alphaeffxx))/(averageradius^3-alphaeffxx);
epseffyy=(hsteps*(averageradius^3+2*alphaeffyy))/(averageradius^3-alphaeffyy);
epseffcart=f*[epseffxx,0,0;0,epseffyy,0;0,0,1]*inv(f);

% return effective eps if plot==1 or polarizations if plot==2
if plot==1
    result=[epseffcart(1,1);epseffcart(2,1)];
else
    result=P;
end
```

```
function result=DAtarget(targetnum,parameter1,parameter2,parameter3,dipolespacing)

% available targets
%   #1: two particles
%           parameter1=axis alignment
%   #2: radially inhomogenous cluster
%           parameter1=cluster_R
%           parameter2=shell_N
%   #3: cubic array
%           parameter1=side_L

if targetnum==1

    if parameter1=='x'
        target_1=[1;1];
    end

    if parameter1=='y'
        target_1=[1,1];
    end

    if parameter1=='z'
        target_1=ones(1,1,2);
    end

end

if targetnum==2

    % Length of grid
    grid_L=floor(2*parameter1/dipolespacing+1);

    % Center of grid
    center=(grid_L+1)/2;
    center_vect=[center;center;center];

    % Length of shells
    shell_L=((grid_L-1)/2)/parameter2;

    % Number of points in shell
    shell_pnts=zeros(parameter2,1);
    x=1;
    y=1;
    z=1;
    while z<=grid_L

        dist=sqrt((x-center_vect(1))^2+(y-center_vect(2))^2+(z-center_vect(3))^2);
        for n = 1:parameter2
            if dist == 0
                shell_pnts(1)=shell_pnts(1)+1;
            end
```

```
            if dist > (n-1)*shell_L & dist <= n*shell_L
                shell_pnts(n)=shell_pnts(n)+1;
            end
        end

        if x==grid_L
            x=1;
            if y==grid_L
                y=1;
                z=z+1;
            else
                y=y+1;
            end
        else
            x=x+1;
        end
    end

    % Shell densities
    for n = 1:parameter2
        density=floor(exp(1-n)*shell_pnts(n));
        if n == 1
            density_array=density;
        else
            density_array=[density_array;density];
        end
    end

    % Total points to fill
    for n = 1:parameter2
        next=density_array(n);
        if n == 1
            particle_N=next;
        else
            particle_N=particle_N+next;
        end
    end

    particle_N=floor(particle_N*(1-(1/4)))
    % Generate grid
    target_1=zeros(grid_L,grid_L,grid_L);

    % Number of points in shell so far
    shell_n=zeros(parameter2,1);

    particle_n=0;
    while particle_n < particle_N
        rnd_pnt=[rnd_gen_1(grid_L);rnd_gen_1(grid_L);rnd_gen_1(grid_L)];
        dist=sqrt((rnd_pnt(1)-center_vect(1))^2+(rnd_pnt(2)-center_vect(2))^2+(rnd_pn↙
t(3)-center_vect(3))^2);
        if target_1(rnd_pnt(1),rnd_pnt(2),rnd_pnt(3))==0;
```

```
            for n = 1:parameter2
                if dist == 0
                    shell=1;
                end
                if dist > (n-1)*shell_L & dist <= n*shell_L
                    shell=n;
                end
                if dist > parameter2*shell_L
                    shell=parameter2;
                end
            end
            if shell_n(shell) < density_array(shell)
                target_1(rnd_pnt(1),rnd_pnt(2),rnd_pnt(3))=1;
                shell_n(shell)=shell_n(shell)+1;
                particle_n=particle_n+1;
            end
        end
    end

end

if targetnum==3
    target_1=ones(parameter1,parameter1,parameter1);
end

% return target
result=target_1;
```

```
function result=rnd_gen_1(length)

rnd=0;
while rnd == 0
    rnd=floor(rand(1)*length);
end

result=rnd;
```

Vita

Damon Smith was born on October 31, 1973 in Leesville, Louisiana and received his B.S. in Physics from the University of New Orleans in 2003. In May 2005, he will receive his M.S. in Applied Physics and will be pursing a Ph.D. in Materials Science and Engineering at the University of Texas at Austin beginning in August 2005.